PROGRESS IN
INORGANIC CHEMISTRY

Edited by

KENNETH D. KARLIN

DEPARTMENT OF CHEMISTRY
JOHNS HOPKINS UNIVERSITY
BALTIMORE, MARYLAND

VOLUME 49

Progress in
Inorganic Chemistry
Volume 49

Advisory Board

PROGRESS IN INORGANIC CHEMISTRY

Edited by

KENNETH D. KARLIN

DEPARTMENT OF CHEMISTRY
JOHNS HOPKINS UNIVERSITY
BALTIMORE, MARYLAND

VOLUME 49

Contents

**Progress in
Inorganic Chemistry**
Volume 49

Nonclassical Metal Carbonyls

ANTHONY J. LUPINETTI and STEVEN H. STRAUSS

Department of Chemistry
Colorado State University
Fort Collins, CO

GERNOT FRENKING

Fachbereich Chemie
Philipps-Universität Marburg
Marburg D-35032, Germany

CONTENTS

I. INTRODUCTION

A. Scope of This Chapter

We will be concerned with the geometric and electronic structures, as probed by spectroscopic, diffraction, and theoretical methods, of M–C≡O and E–C≡O species with ν(CO) values >2143 cm^{-1} (M = a metallic element, E = a nonmetallic element). As discussed in Section II, a ν(CO) value >2143 cm^{-1}, which is the value for gaseous CO, is the most important criterion that categorizes a M–C≡O species as a nonclassical metal carbonyl. Our coverage of the structural and spectroscopic data and theoretical results for this class of compounds, molecular fragments, and surface-bound species will be comprehensive. However, our coverage of the synthetic strategies that have been used to synthesize or generate nonclassical M–CO and E–CO species will be limited to brief comments and to two in-depth case histories.

B. Importance of Metal Carbonyl Compounds in the Chemical Sciences

Carbon monoxide is one of the most important ligands in transition metal chemistry (1–55). Its uses range from a ligand for fundamental studies of structure and bonding to a chemical feedstock. Many industrial processes, including hydroformylation, Fischer–Tropsch synthesis, methanol synthesis, acetic acid synthesis, and the water–gas shift reaction employ CO as a reagent and transition metal compounds as heterogeneous or homogeneous catalysts and involve the intermediacy of metal carbonyls. Carbon monoxide is used to stabilize transition metals in low, even negative, oxidation states. It is also used as a probe ligand in diverse fields such as surface chemistry, catalysis, solid-state chemistry, organometallic chemistry, and biochemistry. The classical picture of metal–carbonyl bonding, shown in Fig. 1, is well developed and is one of the most enduring paradigms in inorganic chemistry. It involves synergistic bonding, with carbon monoxide acting simultaneously as a σ-donor and π-acceptor ligand for d-block metals. The literature of metal carbonyl chemistry is so vast that more than 600 review articles on this subject have appeared since 1967. To provide the reader with an entry point into this literature, most of the important reviews that have appeared in the 1990s are listed

M–CO σ bond

M–CO π bond
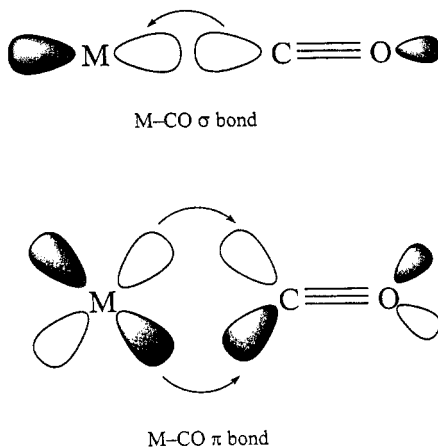
Figure 1.   The classical description of synergistic bonding in metal carbonyls.

as Refs. 1–50 (for convenience, we have included the titles for these references) (1–50). Two other important references are the important monograph by the Olivés, which was published in 1984 (51), and the equally important monograph by Braterman, which was published in 1975 (52). For a glimpse of the field of metal carbonyl chemistry in its earlier years, the reader can consult some of the oldest available reviews (53–55).

C.   Importance of Nonclassical Metal Carbonyls

In addition to their intrinsic interest as "unusual" metal carbonyl species, some nonclassical metal carbonyls, especially those of Groups 10 (VIII), 11 (IB), and 12 (IIB), are of technological importance. Copper(I) and Zn(II) carbonyls may be involved as intermediates in the large-scale industrial transformation of CO to CH_3OH using copper-promoted ZnO catalysts (1, 28, 32, 33, 51, 56). Copper(I) carbonyls may be involved as intermediates in the heterogeneous copper-catalyzed low-temperature water–gas shift reaction (57), and Pd(I), Pd(II), Cu(I), Ag(I), and Au(I) carbonyls may be homogeneous catalysts in the production of carboxylic acids and carbamate esters from alkenes (58–69). Copper(I) carbonyls are formed when CO is absorbed by supported or soluble Cu(I) salts, which are used to remove CO from a variety of industrial gas streams (70–74). In addition, biochemists have long used CO as a probe ligand for the elucidation of structural and dynamic properties of reduced Cu-containing proteins and enzymes, including hemocyanin and cytochrome c oxidase, although in most of these cases $\nu(CO) < 2143$ cm^{-1} (75–79). Perhaps the greatest, if unappreciated, significance of nonclassical metal carbonyls is that they provide a model for a lengthened M–CO bond of a classical metal car-

bonyl (i.e., an M⋯CO bond of a classical metal carbonyl). To our knowledge, no one has studied the reactivity of the CO ligand of a classical, catalytic M–CO species as the M–C distance is lengthened from its equilibrium value, thereby decreasing π back-bonding. In the discussion in Section IV, we will demonstrate that many metal carbonyls that are classical at equilibrium are nonclassical during their formation.

D. Historical Perspective

Despite the recent activity in the area of metal carbonyls with $\nu(CO) > 2143$ cm^{-1} (2, 4, 18–20, 23, 27) it should be noted that metal carbonyls with $\nu(CO) > 2143$ cm^{-1} have been known almost since the inception of metal carbonyl chemistry. Previous workers noted the "atypical" nature of metal carbonyls of late d-block metal ions and suggested that many such compounds have little or no π back-bonding (80–82). The compound Au(CO)Cl, with $\nu(CO) = 2162$ cm^{-1}, was first described in the literature in 1925 (83). Even more striking is cis-Pt(CO)$_2$Cl$_2$, with $\nu(CO)_{ave}$ = 2158 cm^{-1}. The synthesis of this complex, one of only ~250 reported to date with $\nu(CO) > 2143$ cm^{-1}, was reported by Schützenberger in 1870 (84), two decades before Mond (85) reported the synthesis of Ni(CO)$_4$. History is full of ironies, and the history of chemistry is no exception. The first metal carbonyl complex to be reported in the literature was not the prototype: cis-Pt(CO)$_2$Cl$_2$ turned out to be categorically different than ~99% of what was to come.

II. THE JUSTIFICATION FOR TWO CATEGORIES OF METAL CARBONYLS

A. What Is a Classical Metal Carbonyl? The Ten Statements

Listed below are five pairs of statements about transition metal carbonyls that most chemists would agree are unambiguous and valid. It may seem at first that each pair of statements is repetitive, that is, that each pair is simply two ways of expressing the same concept. However, the important distinction between the a Statements (1a–5a) and the b Statements (1b–5b) is that the former are true for all metal carbonyls while the latter (with the possible exception of Statement 4b) are not true for all metal carbonyls (2).

1a. Carbon monoxide (CO) is a σ-donor and a π-acceptor ligand.
1b. M–CO bonds have a significant M←CO σ component and a significant M→CO π component.
2a. The π component (π back-bonding) involves the transfer of electron density from metal d_π orbitals to CO π^* orbitals.

2b. The C–O distances [$R(CO)$] are longer and $\nu(CO)$ values are lower for metal carbonyls than for the free CO molecule (1.12822 Å and 2143 cm^{-1}, respectively).

3a. Adding a donor ligand L to a metal carbonyl complex increases the electron density at the metal center and enhances M→CO π back-bonding.

3b. Adding a donor ligand L to a metal carbonyl complex results in a stronger, shorter M–CO bond and a weaker, longer C–O bond.

4a. Substituting an ancillary ligand L with one that is a stronger σ donor enhances M→CO π back-bonding.

4b. Substituting an ancillary ligand L with one that is a stronger σ donor results in a stronger, shorter M–CO bond and a weaker, longer C–O bond.

5a. The transformation LM(CO)$_n$ → LM(CO)$_{n-1}$ + CO results in fewer π-acceptor CO ligands competing for the same metal d_π electron density.

5b. The transformation LM(CO)$_n$ → LM(CO)$_{n-1}$ + CO results in weaker, longer C–O bonds and lower $\nu(CO)$ values.

Let us consider typical examples for which the Statements 1b–5b are true. The synergistic nature of M–CO bonding, shown in Fig. 1 and discussed at length in Section IV, is very well accepted. Even before the application of molecular orbital (MO) theory to metal complexes, the unexpectedly (for the time) short Ni–CO distance in Ni(CO)$_4$ (86) prompted Pauling to suggest partial double-bond character for the nickel–carbon bonds (87). This was followed by the now standard Dewar-Chatt–Duncansen MO model (88–90). A good example with which to demonstrate the validity of Statement 1b is Cr(CO)$_6$. In 1980, both Sherwood and Hall (91) and Bursten et al. (92) predicted that the amount of Cr→CO π back-bonding in Cr(CO)$_6$ was between 33 and 45% of the amount of Cr←CO σ bonding. The recent predicted value of 35% based on a modern DFT charge decomposition analysis of Cr(CO)$_6$ is consistent with these earlier results (93). A good example to demonstrate the validity of Statement 2b is the tetrahedral complex Co(CO)$_4^-$. The value of $\nu_{asym}(CO)$ for the sodium salt in hexamethylphosphoramide (HMPA) solution is 1890 cm^{-1} (35), more than 250 cm^{-1} below the 2143-cm^{-1} value for free CO. The $R(CO)$ values for the protonated quinuclidine salt of Co(CO)$_4^-$ ($\pm\sigma$ value shown in parentheses) range from 1.154(3) to 1.165(3) Å (94), >0.025 Å longer than the 1.12822-Å value for free CO. Note that the structure of [H(quinuclidine)][Co(CO)$_4$] is one of very few recent structures of metal carbonyls in which $R(CO)$ lengthening was observed to be significant at the $\pm3\sigma$ level of confidence. In the past, X-ray structures of metal carbonyls were rarely of sufficient precision that derived $R(CO)$ values were significantly different than 1.12822 Å. This is a consequence of the strength of the CO bond, which is one of the strongest known chemical bonds. The depth, and hence the steepness, of its potential energy well re-

quires that even a significant change in CO bond energy upon coordination to a metal center will result in only a modest change in $R(CO)$.

A good example to demonstrate the validity of Statement 3b is the addition of two weak F^- ion donors to the linear $Pd(CO)_2$ moiety, which was studied at the MP2 (Moeller–Plesset perturbation theory terminated at second order) level of theory (95). Even with relatively long $Pd–F^-$ distances of 3 Å, the D_{2h} symmetry complex $[Pd(CO)_2F_2]^{2-}$ was predicted to have Pd–C and C–O distances (1.924 and 1.167 Å) that were shorter and longer, respectively, than the corresponding predicted distances in linear $Pd(CO)_2$ (1.942 and 1.156 Å). In harmony with the longer, weaker C–O bonds in $[Pd(CO)_2F_2]^{2-}$, the predicted value of $\nu_{sym}(CO)$ decreased by 66 cm^{-1} on going from linear $Pd(CO)_2$ to D_{2h} $[Pd(CO)_2F_2]^{2-}$. Clearly, the F^- σ-donor ligands induce additional π back-bonding in $[Pd(CO)_2F_2]^{2-}$ relative to $Pd(CO)_2$.

There are many examples that demonstrate the validity of Statement 4b. Two classic examples are the consequences of substituting three CO ligands in $Cr(CO)_6$ with three σ donor ligands. The 1.909(3) Å average Cr–CO distance in $Cr(CO)_6$ decreased to 1.839(4) Å in fac–$Cr(CO)_3(PH_3)_3$ (96) and to 1.816(5) Å in fac–$Cr(CO)_3(NH(C_2H_4NH_2)_2)$ (97).

Three examples that demonstrate the validity of Statement 5b are $Cr(CO)_6$ [$\nu(CO)_{ave} = 2017$ cm^{-1}] versus $Cr(CO)_5$ [$\nu(CO)_{ave} < 2000$ cm^{-1}] (98), $CpMn(CO)_3$ [$\nu(CO)_{ave} = 1967$ cm^{-1}] versus $CpMn(CO)_2$ [$\nu(CO)_{ave} = 1921$ cm^{-1}] (99), and $Fe(OEP)(CO)_2$ [$\nu(CO)_{ave} \geq 2016$ cm^{-1}] versus $Fe(OEP)(CO)$ [$\nu(CO) = 1951$ cm^{-1}] (100).

B. Violations of Statements 1b–5b: Experimental and Theoretical Observations That Led to the Nonclassical Metal Carbonyl Concept

1. $\nu(CO) > 2143$ cm^{-1} and $R(CO) < 1.12822$ Å

There are now more than 250 M–C≡O and E–C≡O species with $\nu(CO) > 2143$ cm^{-1} (101–257). All of them are listed in Tables I–VII and many will be discussed in detail in Sections III and IV. At least nine of these have $R(CO)$ values that are significantly < 1.12822 Å. Two examples that violate both criteria of Statement 2b are $Pd(CO)_2(SO_3F)_2$ [$\nu(CO)_{ave} = 2218$ cm^{-1}; $R(CO) = 1.102(6), 1.114(6)$ Å] (176), shown in Fig. 2, and $Cu(CO)_4^+$ [$\nu_{asym}(CO) = 2184$ cm^{-1}; $R(CO) = 1.109(4) – 1.114(3)$ Å] (212), the structure of which is compared with the structure of $Co(CO)_4^-$ in Fig. 3. The data in Tables I–VII provide compelling evidence that the diatomic molecule CO *can respond in two completely different ways* when it binds to a metal center. In the vast majority of cases, the response is that $R(CO)$ increases and $\nu(CO)$ decreases. This large category of metal carbonyls could be called common, ordinary, or usual; we have chosen to call it classical. Strictly speaking, we should say that metal carbonyls in this category are classical with respect to State-
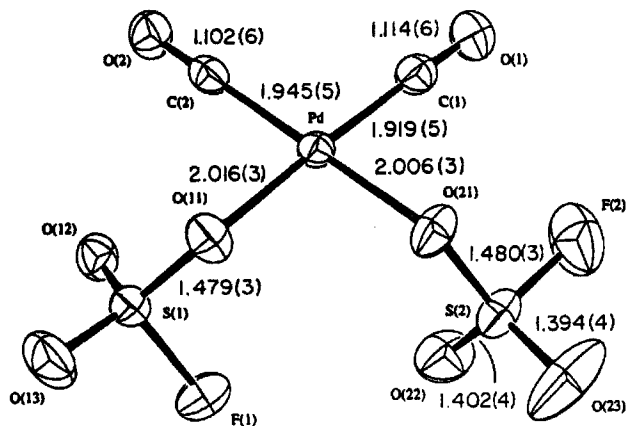
Figure 2.   Structure of *cis*-Pd(CO)$_2$(SO$_3$F)$_2$. [Reprinted with permission from C. Wang, H. Willner, M. Bodenbinder, R. J. Batchelor, F. W. B. Einstein, and F. Aubke, *Inorg. Chem., 33*, 3521 (1994). Copyright © 1994 American Chemical Society.]
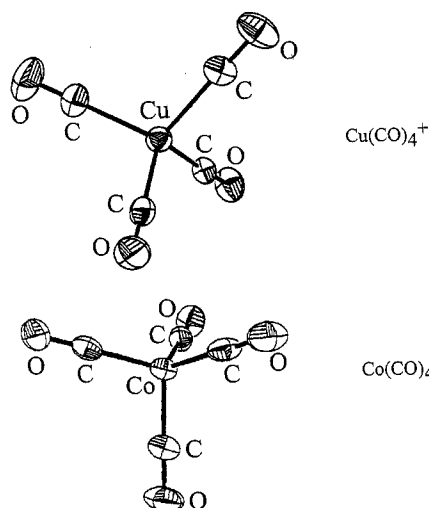
Figure 3.   Structures of the Cu(CO)$_4^+$ cation in Cu(CO)$_4$(1-Et-CB$_{11}$F$_{11}$) (212) and the Co(CO)$_4^-$ anion in [H(quinuclidine)][Co(CO)$_4$] (94). Selected bond distances (Å) and angles (deg): Cu–C, 1.961(3) –1.968(3); C–O, 1.109(4) – 1.114(3); C–Cu–C, 104.3(1) – 112.1(6); O–C–Cu, 174.8(3) – 178.4(3); Co–C, 1.757(2) – 1.777(2); C–O, 1.150(2) – 1.153(2); C–Co–C, 107.5(2) – 113.6(1).

ment 2b. The other response is that $R(CO)$ decreases and $\nu(CO)$ increases, and we call metal carbonyls in this category nonclassical with respect to Statement 2b.

2. Sign of $\Delta R(CO)$ Upon Lengthening $R(MC)$ from $R(MC)_{eq}$

Figure 4 shows the results of recent computational work on $Cu(CO)^+$ and $Ag(CO)^+$ (257). It can be seen that an infinitesimal increase in $R(MC)$ from its equilibrium position results in a shortening of the C–O bond in $Cu(CO)^+$ but a lengthening of the C–O bond in $Ag(CO)^+$. The same perturbation has produced two different responses, classical, $Cu(CO)^+$, and nonclassical, $Ag(CO)^+$.

3. Sign of $\Delta\nu(CO)$ Upon Dissociation of One CO Ligand from a Polycarbonyl Complex

Experimental $\nu_{asym}(CO)$ values for $Cu(CO)_3(AsF_6)$ and $Cu(CO)_2(AsF_6)$ are 2179 and 2164 cm^{-1}, respectively, in harmony with Statement 5b (200). In contrast, $\nu_{asym}(CO)$ values for $Ag(CO)_3(Nb(OTeF_5)_6)$ and $Ag(CO)_2(Nb(OTeF_5)_6)$ are 2191 and 2198 cm^{-1}, respectively, in violation of Statement 5b (148, 220). In this case too, the same perturbation, loss of a ligand, has produced two different responses, classical (Cu^+) and nonclassical (Ag^+). Note that the copper complexes behave classically with respect to Statement 5b but nonclassically with respect to Statement 2b.
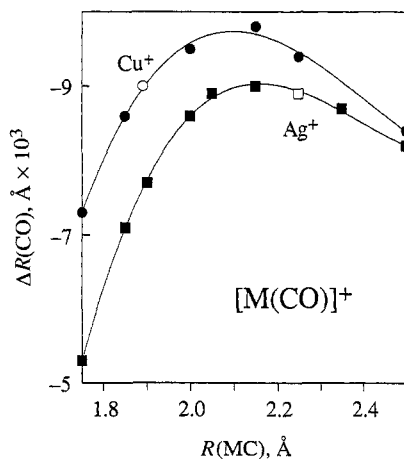
Figure 4. Plots of $\Delta R(CO)$, the change in carbon–oxygen distance, versus $R(MC)$, the metal–carbon distance, for the monocarbonyls $Cu(CO)^+$ and $Ag(CO)^+$ (MP2 level of theory). The open data points represent the equilibrium geometry. Note that at the equilibrium geometry, the C–O bonds in both $Cu(CO)^+$ and $Ag(CO)^+$ are predicted to be –0.009 Å shorter than in free CO. The data are from (256).

4. $M(CO)_n^+$ versus $M(CO)_nF_2^-$

When M^+ is Cu^+, the addition of two F^- ions at 3 Å along the perpendicular to the bond axis through Cu^+ in linear $Cu(CO)_2^+$ resulted in a $\nu(CO)$ decrease of 32 cm^{-1} and a $R(CuC)$ *decrease* of 0.034 Å, in harmony with Statement 3b (95). In contrast, when M^+ is Ag^+, the addition of two F^- ions resulted in a $R(AgC)$ *increase* of 0.036 Å (95). Once again, the same perturbation has produced two different effects, classical (Cu^+) and nonclassical (Ag^+), as shown in Fig. 5. Interestingly, the addition of two F^- ions to $Ag(CO)_2^+$ also resulted in a $\nu(CO)$ decrease of 32 cm^{-1}. As above, the copper complexes behave classically with respect to Statement 3b but nonclassically with respect to Statement 2b [i.e., the $\nu(CO)$ values and the $R(CO)$ values for both copper complexes are higher than and smaller than, respectively, the corresponding parameters for gaseous CO].

C.   What Is a Nonclassical Metal Carbonyl

Some of the results listed above for copper(I) carbonyls might be thought of as confusing, at least at first glance. For example, are $Cu(CO)_3(AsF_6)$ and $Cu(CO)_2(AsF_6)$ classical or nonclassical? The answer is that it depends on which statement about metal carbonyls is being considered. These two complexes are nonclassical with respect to Statement 2b, but they are classical with respect to Statement 5b. This apparent confusion does not, in our opinion, diminish the usefulness of the classical–nonclassical distinction. That the phrase *with respect to* is needed to answer the question should be no more disconcerting than the fact that this three-word phrase is also needed to answer questions unambiguously about the
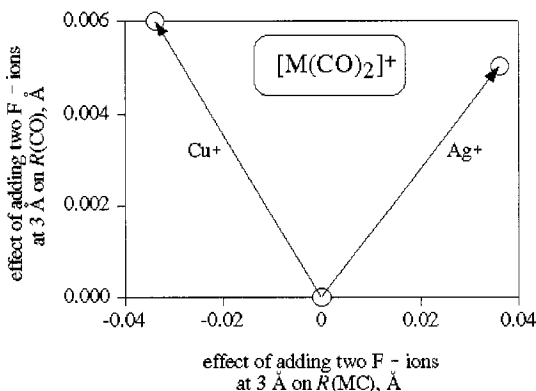
Figure 5.   The predicted effects of adding two F^- ions to the linear d^{10} complexes $Cu(CO)_2^+$ and $Ag(CO)_2^+$. The data are from (95).

stability of compounds. For example, a compound might be thermodynamically *stable* with respect to its constituent elements but *unstable* with respect to disproportionation or with respect to another set of products. As far as a simple question of stability is concerned, the most sensible approach is to designate a compound as unstable if it is unstable with respect to *at least one* set of products, even if it is stable with respect to other possible sets of products. Accordingly, we believe that the most sensible way to label metal carbonyls is as follows: metal carbonyls that conform to Statements 1b–5b are classical metal carbonyls; any metal carbonyl complex that violates *at least one* of Statements 1b–5b is a nonclassical metal carbonyl. Even if a complex violates only one of the five statements, its designation as nonclassical serves to alert other scientists that it is an unusual compound and that careful scrutiny of it might be rewarded with new chemical insights and discoveries.

III. SURVEY OF NONCLASSICAL METAL CARBONYLS AND RELATED SPECIES

In this section, we list in Tables I–VII all known species with M–C≡O or E–C≡O linkages for which ν(CO) is >2143 cm^{-1} (101–257). Our coverage of CO adducts of metal oxides and halides is representative, not exhaustive. For example, there are more than a dozen papers reporting vibrational spectra of CO on MgO crystallites, but only two are listed in Table I. The reader should consult the excellent and up-to-date review by Zecchina et al. (1) for a comprehensive treatment of this important literature.

We also list in Table VIII those species that have also been characterized by ^{13}C NMR spectroscopy (258–263). We have included a few relevant species with ν(CO) < 2143 cm^{-1} for comparison. The E–CO entries include species with CO bonded to nonmetallic electrophiles such as H$^+$, HF, BH$_3$, CH$_3^+$, N$^+$, and Cl$^+$. There are now >250 carbonyl species with average ν(CO) values >2143 cm^{-1}. This can be compared with the very large number of metal carbonyls that have been reported in the literature between the years 1870 and 1999. In 1985, there were 10,022 R(CO) values in the Cambridge Structural Database (CSD) for which the M–C–O bond angle was ≥173° (264). The "average" metal carbonyl complex in the database undoubtedly has more than one CO ligand. However, considering that the CSD analysis included only terminal carbonyls and only metal carbonyl complexes that had been structurally characterized and that contain one or more C–H bonds, the total number of metal carbonyl species that have been studied to date is probably >10,000 and may be as high as 20,000. Hence, nonclassical metal carbonyls probably number ~1–2% of the total.

TABLE I

s-Block M–CO Species With $\nu(CO) > 2143$ cm^{-1}

M	Species without CO	Conditions	$\nu(CO)^a$ (cm^{-1})	References
H$^+$	H$^+$	Gas phase	2184	101,102
	HF/SbF$_5$	Superacid soln	2110	103
	HF	Photofragmentation of matrix isolated FCHO, 20 K	2162	104
	HF	14 K; Ar/CO matrix	2159	105
	HCl	20 K; Ar/CO matrix	2156	106
	X$_3$SiOH	100 K; Na- and Al-free silicalite S	2156	107
	H(ZSM-5)	226 K; zeolite–ZSM-5	2173	108
Li$^+$	LiF	10 K; Ar/CO matrix	2185	109
		77 K; 100 face, two sites	2177, 2155	111
	Li$_2$F$_2$	10 K; Ar/CO matrix	2176, 2173, 2168	109
	Li(ZSM-5)	226 K (77 K); zeolite–ZSM-5	2185 (2188)^b	108,112,113
Na$^+$	NaF	10 K; Ar/CO matrix	2172	109
	Na$_2$F$_2$	10 K; Ar/CO matrix	2155	109
	NaCl	5 K; 100 face	2155	115,116
		77 K; 100 face	2159	111
	NaI	77 K; 100 face	2160	111
	Na(MOR)	77 K; MOR = zeolite–mordenite	2177	118
	Na(ZSM-5)	226 K (77 K); zeolite–ZSM-5	2170 (2178)^b	108,118
	Na(Y)	77 K; Y = Union Carbide zeolite–LZY-52	2170	119
	Na,Rb(Y)	110 K; Y = Enichem zeolite (Si/Al = 2.7)	2166	120
	Na(L)	77 K; L = zeolite–LTL, two sites	2174, 2157	121
	Na(A)	130 K; A = Linde 4 Å zeolite–A	2155	122
	Na(ETS-10)	100 K; ETS-10 = titanosilicate molecular sieve	2176	123
	Na(CO)(ETS-10)	100 K; ETS-10 = titanosilicate molecular sieve	2164	123
K$^+$	KCl	77 K; 100 face, low coverage	2153	111
	K(MOR)	77 K; MOR = zeolite–mordenite	2163	118
	K(ZSM-5)	226 K (77 K); zeolite–ZSM-5	2161 (2162)^b	108,118
	K(L)	77 K; L = zeolite–LTL, two sites	2161, 2150	121
	K(ETS-10)	100 K; ETS-10 = titanosilicate molecular sieve	2168, 2162	123
Rb$^+$	Rb(MOR)	77 K; MOR = zeolite–mordenite	2159	118
	Rb(ZSM-5)	226 K (77 K); zeolite–ZSM-5	2158 (2162)^b	108,118
	Na,Rb(Y)	111 K; Y = Enichem zeolite (Si/Al = 2.7)	2157	120
Cs$^+$	Cs(MOR)	77 K; MOR = zeolite–mordenite	2155	118
	Cs(ZSM-5)	226 K (77 K); zeolite–ZSM-5	2145 (2157)^b	108,118
Be^{2+}	BeO	77 K	2207, 2200, 2188	124
Mg^{2+}	MgF$_2$	10 K; Ar/CO matrix	2176, 2173, 2168	109
	MgO	77 K; 001 face, low coverage, three sites	2203, 2170, 2157	125
		77 K; 100 face, low coverage, two site	2170, 2157	111
	Mg(Y)	77 K; zeolite–Y	2213	126

TABLE I (*Continued*)

M	Species without CO	Conditions	$\nu(CO)^a$ (cm^{-1})	References
	Mg(X)	77 K; zeolite–X	2205	126
Ca^{2+}	CaF$_2$	matrix isolated	2187, 2180	105,109
	Ca(Y)	77 K; zeolite–Y	2197, 2198	112,113,126
	Ca(X)	77 K; zeolite–X	2192	126
	CaO/Al$_2$O$_3$	3% CaO, 300 K	2182	110
	Ca(Cp*)$_2$	Toluene soln	2158	127
Sr^{2+}	SrF$_2$	10 K; Ar/CO matrix	2181, 2174, 2166	109
	Sr(Y)	77 K; zeolite–Y	2186	126
	Sr(Cp*)$_2$	Toluene soln	2159	127
Ba^{2+}	BaF$_2$	10 K; Ar/CO matrix	2173, 2164, 2160	109
	Ba(Y)	77 K; zeolite–Y	2178	126
	Ba(X)	77 K; zeolite–X	2172	126

^{a}The $\nu(CO)$ values are from IR spectra.
^{b}The value in parentheses corresponds to the temperature in parentheses in the conditions column.

A. s-Block Species

1. H$^+$

The gas-phase linear triatomic cation HCO$^+$ [$\nu(CO) = 2184$ cm^{-1}] (101, 102) has not yet been isolated as a simple salt, probably because its superacidic nature is not compatible with any anion used to date. Nevertheless, a great deal is known about this important species, the first polyatomic ion detected in interstellar space (265, 266) and possibly the most abundant ion in hydrocarbon flames (267). There is a recent report of the IR spectrum of solvated HCO$^+$ in the neat superacid HF/SbF$_5$, with $\nu(CO) = 2110$ cm^{-1} (103). This value seems rather low, considering the $\nu(CO)$ values of matrix isolated FH–CO and ClH–CO, which are ≥ 2156 cm^{-1} (104–106). There is a report of a Si–O–H–CO species that was formed in a sodium- and aluminum-free silicalite with $\nu(CO) = 2156$ cm^{-1} (107). There is also a report of an HCO$^+$ like species with $\nu(CO) = 2173$ cm^{-1}, which was formed when the acidic zeolite H(ZSM-5) was placed under a CO atmosphere (108).

2. Li$^+$ to Cs$^+$

There are no molecular MCO$^+$ species known for M$^+$ = Li$^+$–Cs$^+$. All of the species listed in Table I were generated by adding CO to alkali metal halide surfaces or to alkali metal substituted zeolites. Note that for the mordenite (MOR) and ZSM-5 series of zeolites, $\nu(CO)$ decreases as the ionic radius of the alkali metal increases, as shown in Fig. 6. Note also that $\nu(CO)$ decreases as the Si/Al content of

TABLE II

p-Block M–CO Species With $\nu(CO) > 2143$ cm^{-1}

M	Compound or Species	$\nu(CO)^a$ (cm^{-1})	$R(MC)$ (Å)	$R(CO)$ (Å)	References
B	$BH_3(CO)$	2167 (Ne matrix, 10 K)	1.53(1)	1.135(10)	128–130
	$B_2H_4(CO)_2$	2153	1.52(1)	1.125(7)	131
	$B_3H_7(CO)$	2203	1.54(1)	1.11(1)	132
	$B_4H_8(CO)$	2150			133
	$B_4F_6(CO)$	2162			134
	$1,10\text{-}B_{10}Cl_8(CO)_2$	2203			135
	$1,10\text{-}B_{10}H_8(CO)_2$	2147			135
	$1\text{-}SMe_2\text{-}6\text{-}B_{10}H_8(CO)$	2157			135
	$[PMePh_3][2\text{-}B_{10}H_9(CO)]$	2129	1.484(6)	1.130(5)	137
	$1,7\text{-}B_{12}H_{10}(CO)_2$	2223			135
	$1,12\text{-}B_{12}H_{10}(CO)_2$	2210	1.543(2)	1.119(2)	135,136
	$1\text{-}NMe_3\text{-}12\text{-}B_{12}H_{10}(CO)$	2204			135
	$[NMe_4][B_{12}H_{11}(CO)]$	2178			135
Al^{3+}	$AlMe_3(CO)$ (neat CO matrix)	2185			138
	$Al_2O_3 + CO$	2238–2150			110, 124, 139–142
R^+	CH_3CO^+/H_2SO_4	2309			143
	$[CH_3CO][SbF_6]$	2294	1.38(2)	1.116(21)	144, 145
	$[CH_3CO][SbCl_6]$	2295	1.45(2)	1.109(30)	146, 147
	$[(CH_3)_2CHCO][SbCl_6]$	2257	1.458(4)	1.101(4)	148
	$[1,4\text{-}C_6H_4(CH_3)CO][SbCl_6]$		1.40(1)	1.097(9)	149
Si^{4+}	$SiO_2(CO)$	2158			124
Sn^{2+}	$Sn(CO)Cl_2$ (Ar matrix)	2176			150
Pb^{2+}	$Pb(CO)F_2$ (Ar matrix)	2176			150
	$Pb(CO)Cl_2$ (Ar matrix)	2175			150
	$Pb(CO)Br_2$ (Ar matrix)	2161			150
	$Pb(CO)I_2$ (Ar matrix)	~2149			150
N^+	$[N(CO)_2][Sb_3F_{16}]$	2366, 2287	C–N–C = 130.7(3)	1.118(4), 1.114(5)	151
Cl^+	$[ClCO][Sb_nF_{5n+1}]$ ($n > 2$)	2256			152, 153

^{a}The $\nu(CO)$ values in italics are from Raman spectra; all other $\nu(CO)$ values are from IR spectra.

14

TABLE III

Groups 3 (IIIB)–7 (VIIB) M–CO Species With $\nu(CO) > 2143$ cm^{-1}

M	Species (conditions)	$\nu(CO)$ (cm^{-1})	References
Sc^{3+}	Sc(CO)O$^+$ (12 K, Ar matrix)	2222	154a
	Sc(CO)F$_3$ (10 K; Ar/CO matrix)	2212, 2208	109
	Sc$_2$(CO)F$_6$ (10 K; Ar/CO matrix)	2204	109
Y^{3+}	Y(CO)O$^+$ (12 K, Ar matrix)	2206	154a
	Y(CO)F$_3$ (10 K; Ar/CO matrix)	2198	109
	Y$_2$(CO)F$_6$ (10 K; Ar/CO matrix)	2184	109
La^{3+}	La(CO)F$_3$ (10 K; Ar/CO matrix)	2182	109
	La$_2$(CO)F$_6$ (10 K; Ar/CO matrix)	2119[a]	109
	La$_2$O$_3$ + CO (77 K)	2170	255, 256
Ti^{3+}	Ti(CO)O$^+$ (Ar matrix, 12 K)	2188	154b
Ti^{4+}	TiO$_2$ (rutile) + CO	2182	156
	TiO$_2$ (anatase) + CO	2212–2178	124, 157, 158
	TiO$_2$/SiO$_2$ + CO	2188–2180	158
Zr^{4+}	ZrO$_2$ + CO	~2190	159
	sd-ZrO$_2$ (H$_2$SO$_4$ surface loading)	2220–2170	159
	O-outside-Zr(CO)(Cp*)$_2$(COCH$_3$)(Z)/CH$_2$Cl$_2$[b]	2105	160
	O-inside-Zr(CO)(Cp*)$_2$(COCH$_3$)(Z)/CH$_2$Cl$_2$[b]	2152	160
	O-outside-Zr(CO)(Cp)$_2$(COCH$_3$)(Z)/CH$_2$Cl$_2$[b]	2123	160
	O-inside-Zr(CO)(Cp)$_2$(COCH$_3$)(Z)/CH$_2$Cl$_2$[b]	2176	160
V^{3+}	V(CO)O$^+$ (12 K; Ar matrix)	2205	154b
Cr^{2+}	Cr(CO)F$_2$ (matrix isolated)	2185	105
Cr^{3+}	Cr(CO)O$^+$ (12 K; Ar matrix)	2176	155
	Cr$_2$O$_3$ + CO	2184	156
	Cr$_2$O$_3$ (01$\bar{1}$2 face) + CO	2181	125, 161
	Cr$_2$O$_3$ (11$\bar{2}$0 face) + CO	2158	125, 161
Mn^{2+}	Mn(CO)F$_2$ (matrix isolated)	2183	105
	Mn(zeolite–Y) + CO	2208	126
	Mn(zeolite–X) + CO	2203	126
Mn^{3+}	Mn(CO)O$^+$ (12 K; Ar matrix)	2173	155

[a] This may be a typographical error in the original report.
[b] Here Z$^-$ = B(CH$_3$)(C$_6$F$_5$)$_3^-$.

the zeolite increases (the Si/Al content increases in the order zeolite–MOR < zeolite–ZSM-5 < zeolite–Y < zeolite–L < zeolite–A), as shown in Fig. 7. In most cases, there is a 5–15 cm^{-1} shift to lower energy as coverage increases. For this reason, the $\nu(CO)$ values listed in Table I are, whenever possible, for low coverage or are extrapolated to zero coverage. With one exception, all of the carbonyl species in Table I are monocarbonyls. The exception is the recently reported sodium dicarbonyl, Na(CO)$_2$(ETS-10), species, where ETS-10 is a titanosilicate molecular sieve (121).

TABLE IV

Groups 8 (VIII), 9 (VIII), and 10 (VIII) M—CO Species With ν(CO) > 2143 cm^{-1}

M	Compound or Species	ν(CO)^a (cm^{-1})	R(MC) (Å)	R(CO) (Å)	References
Fe^{2+}	Fe(CO)(zeolite–Y)	2198			126
Fe^{3+}	Fe(CO)$_6$(Sb$_2$F$_{11}$)$_2$	2241(s), 2220(m), 2204	1.910(5)–1.912(5)	1.102(5)–1.107(5)	162,163
	Fe$_2$O$_3$ + CO (77 K)	2165			125
Ru^{2+}	Ru(CO)$_6$(Sb$_2$F$_{11}$)$_2$	2254(s), 2222(m), 2199			164
Os^{2+}	Os(CO)$_6$(Sb$_2$F$_{11}$)$_2$	2259(s), 2218(m), 2190			164
Co$^+$	Co(CO)$^+$ in Ne/CO matrix	2166			165,166
	Co(CO)$_2^+$ in Ne/CO matrix	2169			165,166
	Co(CO)$_4$(L)$^+$/HSO$_3$F^{b,c}	2194(s), 2155(m), 2139, 2122			167
Co^{2+}	Co(CO)O	2179			168
	Co(CO)(zeolite–Y)	2208			126
	Co(CO)(zeolite–X)	2204			126
Rh$^+$	Rh(CO)$^+$ in Ne/CO matrix	2174			165,166
	Rh(CO)$_2^+$ in Ne/CO matrix	2185			165,166
	Rh(CO)$_3^+$ in Ne/CO matrix	2168			165,166
	Rh(CO)$_4^+$ in Ne/CO matrix	2162			165,166
	Rh(CO)$_4$(zeolite–Y)	2152, 2135, 2124, 2112			251
	Rh(CO)$_2$(NO)(zeolite–Y)	2162, 2128 [ν(NO) = 1786]			252
	Rh(CO)$_2$/HSO$_3$F^b	2216, 2178, 2141			167,172
	[Rh(CO)$_4$][1-Et-CB$_{11}$F$_{11}$]	2215, 2176, 2138	1.947(6)–1.958(6)	1.109(7)–1.124(7)	171
Rh^{3+}	Rh(CO)(polystyrenesulfonate)	2178			253
	NaRh(CO)(zeolite–Y)	2172, 2138			254
	Rh(CO)(zeolite–Y)	2172, 2138			254
	Rh(CO)(zeolite–mordenite)	2175, 2140			254
	Rh(CO)(zeolite–ZSM-34)	2188, 2140			254
	Rh(CO)(zeolite–ZSM-11)	2184, 2150			254
Rh^{4+}	Rh(CO)(O)$_2$/Al$_2$O$_3$	2156			169

(continues)

Ir⁺	Ir(CO)⁺ in Ne/CO matrix	2157			165,166
	Ir(CO)₂⁺ in Ne/CO matrix	2154			165,166
	[Ir(CO)₄][AlCl₄]	2216, 2170, 2125			172
Ir³⁺	IrCl(CO)₅(Sb₂F₁₁)₂	2295(s), 2276(m), 2254	2.02(2)	1.08(2)	173
	Ir(CO)₆(Sb₂F₁₁)₃				173
	mer-Ir(CO)₃(SO₃F)₃	2249(w), 2208(s), 2198(s)	1.937(7), 1.999(6), 2.006(6)	1.094(8), 1.108(8), 1.114(8)	174
	mer-Ir(CO)₃(SO₃F)₃/HSO₃F	2253(s), 2208(m), 2197(m)			174
	fac-Ir(CO)₃(SO₃F)₃/HSO₃F	2233(s), 2157(w)			174
Ni²⁺	NiO + CO	2152			111
	Ni(CO)F₂ (matrix isolated)	2200			105
	Ni₂(CO)F₄ (matrix isolated)	2179			105
	Ni(CO)Cl₂ (matrix isolated)	2189			105
	Ni(CO)(zeolite–Y)	2217			126
	Ni(CO)(zeolite–X)	2211			126
Pd⁺	Pd₂(CO)₂²⁺/H₂SO₄ᵇ	2167, 2144			63
Pd²⁺	[N(n-Bu)₄][Pd(CO)Cl₃]/CH₂Cl₂	2146			178
	cis-Pd(CO)₂(C₆Cl₅)₂	2173, 2152			180
	cis-Pd(CO)₂(C₆F₅)₂	2186, 2163			180
	cis-Pd(CO)₂(SO₃F)₂	2228, 2208	1.945(5), 1.919(5)	1.102(6), 1.114(6)	176,177
	trans-Pd(CO)₂(SO₃F)₂	2212, 2166			177
	Pd₂(μ-CO)₂(CO)₂(SO₃F)₄	2179 (terminal), 1967 (bridging)			176
	Pd₂(CO)₂(μ-Cl)₂Cl₂/toluene	2167, 2160			178–180
Pt⁺	Pd(CO)₄(Sb₂F₁₁)₂	2279(s), 2263(m), 2248	ave = 1.992(2)	ave = 1.106(6)	181,182
	Pt₂(CO)₆²⁺/H₂SO₄ᵈ	2233, 2209, 2195, 2186, 2174			183
	Pt₂(CO)₂Cl₄	2146			178,179
Pt²⁺	cis-Pt(CO)₂I₂/C₂H₂Cl₄	2150, ~2111			184
	cis-Pt(CO)₂Br₂/C₂H₂Cl₄	2170, 2130			184
	cis-Pt(CO)₂Cl₂/C₂H₂Cl₄	2179, 2136	1.901(5), 1.893(5)	1.110(7), 1.121(6)	178,184,185
	cis-Pt(CO)₂Cl₂/SOCl₂	2177, 2136			178
	cis-Pt(CO)₂(C₆Cl₅)₂	2160, 2126			180
	cis-Pt(CO)₂(C₆F₅)₂	2174, 2143			180

(continues)

17

TABLE IV (*Continued*)

M	Compound or Species	ν(CO)[a] (cm^{-1})	R(MC) (Å)	R(CO) (Å)	References
	cis-Pt(CO)$_2$(SO$_3$F)$_2$	2219, 2185			177
	trans-Pt(CO)$_2$Cl$_2$/SOCl$_2$	2160			184
	trans-Pt(CO)$_2$(SO$_3$F)$_2$	*2191, 2145*			177
	Pt(CO)$_4$(Sb$_2$F$_{11}$)$_2$	*2289*(s), 2267(m), 2244	ave = 1.982(9)	ave = 1.110(9)	181,182
	Pt(CO)$_4$(Pt(SO$_3$F)$_6$)	*2281*(s), 2267(m), 2235			186
	Pt(CO)(dfepe)(CF$_3$SO$_3$)+/CF$_3$SO$_3$H[e]	2210			187
	Pt(CO)(dfepe)(SO$_3$F)+/HSO$_3$F[e,f]	2212			187
	Pt(CO)(dfepe)(CH$_3$)+/CF$_3$SO$_3$H[e]	2174			187
	Pt(CO)$_2$(dfepe)+/CF$_3$SO$_3$H[e]	2235, 2221			187
Pt^{4+}	[N(n-Bu)$_4$][Pt(CO)Cl$_5$]	2184			188

[a] The ν(CO) values in italics are from Raman spectra; all other ν(CO) values are from IR spectra.

[b] The counteranion is probably H(SO$_3$F)$_2^-$.

[c] This carbonyl species apparently has a five-coordinate trigonal bipyramidal structure with one equatorial position occupied by a weak ligand L (solvent or anion); the Raman band at 2155 cm^{-1} was also observed in the IR spectrum; the two IR bands were also observed in the Raman spectrum.

[d] The counteranion is probably H(HSO$_4$)$_2^-$; the Raman spectrum also exhibited bands at 2195 and 2174 cm^{-1}.

[e] 1,2-bis(bis(pentafluoroethyl)phosphino)ethane = dfepe; the counteranion is probably H(CF$_3$SO$_3$)$_2^-$.

[f] The counteranion is probably H(SO$_3$F)$_2^-$.

18

TABLE V

Group 11 (IB) M–CO Species With $\nu(CO) > 2143$ cm^{-1}

M	Compound or Species[b]	$\nu(CO)^a$ (cm^{-1})	$R(MC)$ (Å)	$R(CO)$ (Å)	References
Cu$^+$	Cu(CO)$^+$ in Ar/CO matrix	2174			189
	Cu(CO)$^+$ in Ne/CO matrix	2234			189
	Cu(CO)$_2^+$ in Ne/CO matrix	2230			189
	Cu(CO)$_3^+$ in Ne/CO matrix	2211			189
	Cu(CO)$_4^+$ in Ne/CO matrix	2202			189
	Cu(CO)(Tp^f)	2137	1.808(4)	1.110(5)	190
	Cu(CO)Cl	2127	1.86(2)	1.11(2)	191,192
	Cu(CO)Cl (matrix isolated)	2157			193
	(Cu(CO))$_2$O	2127			194
	(Cu(CO)$_2$)$_2$O	2158(m), 2113(s)			194
	(Cu(CO))$_2$O/SiO$_2$	2132			194
	(Cu(CO)$_2$)$_2$O/SiO$_2$	2162, 2120			194
	(Cu(CO))$_2$O/zeolite–MCM-41	2159			195
	(Cu(CO)$_2$)$_2$O/zeolite–MCM-41	2180, 2152			195
	(Cu(CO)$_3$)$_2$O/zeolite–MCM-41	2194, 2171, 2138^c			195
	Cu(CO)(SO$_3$F)/HSO$_3$F soln	2149, 2152			196,198
	Cu(CO)$_4$(SO$_3$F)/HSO$_3$F soln	2181, 2183			196,198
	Cu(CO)(AsF$_6$)	2178			199,200
	Cu(CO)$_2$(AsF$_6$)	2177, 2164			200
	Cu(CO)$_3$(AsF$_6$)	2206(s), 2183(m), 2179			200
	Cu(CO)(CF$_3$SO$_3$)	2133			201
	Cu(CO)$_2$(CF$_3$SO$_3$)	2171(m), 2143(s)			201b
	Cu(CO)(N(SO$_2$CF$_3$)$_2$)	2162			202
	Cu(CO)$_2$(N(SO$_2$CF$_3$)$_2$)	2184(m), 2158(s)	1.895(6), 1.906(6)	1.130(7), 1.115(7)	202
	Cu(CO)$_3$(N(SO$_2$CF$_3$)$_2$)	2190(m), 2172(s)			202
	Cu(CO)(zeolite–Y)	2160			203,204
	Cu(CO)$_2$(zeolite–Y)	2178(m), 2150(s)			203,204
	Cu(CO)(zeolite–M)	2157			204

19

TABLE V (*Continued*)

M	Compound or Species[b]	$\nu(CO)^a$ (cm^{-1})	$R(MC)$ (Å)	$R(CO)$ (Å)	References
	Cu(CO)$_2$(zeolite–M)	2177(m), 2150(s)			204
	Cu(CO)(zeolite–L)	2148			204
	Cu(CO)(zeolite–ZSM-5)	2157			205
	Cu(CO)$_2$(zeolite–ZSM-5)	2178(m), 2151(s)	1.95(5)		205, 206
	Cu(CO)$_3$(zeolite–ZSM-5)	2192(m), 2167(s)	1.93(2)		205, 207
	Cu(CO)(NH$_3$)(zeolite–ZSM-5)	2098			206
	Cu(CO)$_2$(NH$_3$)(zeolite–ZSM-5)	2158(m), 2128(s)			206
	Cu(CO)(H$_2$O)(zeolite–ZSM-5)	2130			206
	Cu(CO)(zeolite–MFI)	2158			208
	Cu(CO)$_2$(zeolite–MFI)	2177(m), 2151(s)			208
	Cu(CO)$_2$(zeolite–MOR)	2160			209,210
	Cu(CO)$_2$(zeolite–MOR)	2177(m), 2153			209,210
	Cu(CO)$_3$(zeolite–MOR)	2190(sh, m), 2165(sh, s)			210
	Cu(CO)$_2$(OC(CF$_3$)$_3$	2156(m), 2132(s)			211
	Cu(CO)(Al(OCPh(CF$_3$)$_2$)$_4$)	2155			211
	Cu(CO)$_2$(Al(OCPh(CF$_3$)$_2$)$_4$)	2178(m), 2151(s)			211
	Cu(CO)(12-CB$_{11}$H$_{11}$F)	2168(s), 2163(s)			211
	Cu(CO)$_2$(12-CB$_{11}$H$_{11}$F)	2183(m), 2163(s)			211
	Cu(CO)$_2$(1-Bn-CB$_{11}$F$_{11}$)	2184(m), 2166(s)	1.915(3), 1.916(3)	1.109(3), 1.115(3)	212
	Cu(CO)$_3$(1-Bn-CB$_{11}$F$_{11}$)	2190(m), 2172(s)			212
	Cu(CO)$_4$(1-Bn-CB$_{11}$F$_{11}$)	2185			212
	Cu(CO)(1-Et-CB$_{11}$F$_{11}$)	2178			212
	Cu(CO)$_2$(1-Et-CB$_{11}$F$_{11}$)	2187(m), 2173(s)			212
	Cu(CO)$_3$(1-Et-CB$_{11}$F$_{11}$)	2189(m), 2168(s)			212
	Cu(CO)$_4$(1-Et-CB$_{11}$F$_{11}$)	2184	1.961(3)–1.968(3)	1.109(4)–1.114(3)	212
	Cu(CO)F^d	2146			213
Cu^{2+}	Cu(CO)F$_2$ (matrix isolated)	2210			105
	Cu^{II}(CO)(ZSM-5)	2175			204

20

Ag^+	$Ag(CO)(CoCp(POEt_3)_3)$	2125			214
	$Ag(CO)(O_2)$	2165			215
	$Ag(CO)(Tp')$/hexane soln	2162	2.037(5)	1.116(7)	216
	$Ag(CO)(SbF_6)$	2185			217
	$Ag(CO)(OTeF_5)$	2793, 2189			148
	$Ag(CO)(B(OTeF_5)_4)$	2204	2.10(1)	1.077(16)	148,218
	$Ag(CO)_2(B(OTeF_5)_4)$	2198	2.06(5)–2.20(4)	1.07(5)–1.09(6)	148,219
	$Ag(CO)(Nb(OTeF_5)_6)$	2206, 2204			148
	$Ag(CO)_2(Nb(OTeF_5)_6)$	2220, 2198			148
	$Ag(CO)_3(Nb(OTeF_5)_6)$	2191			220
	$(Ag(CO))_2(Zn(OTeF_5)_4)$	2203			148
	$(Ag(CO)_2)_2(Zn(OTeF_5)_4)$	2197			148
	$(Ag(CO))_2(Ti(OTeF_5)_6)$	2207			148
	$(Ag(CO)_2)_2(Ti(OTeF_5)_6)$	2197			148
	$Ag(CO)_2(SO_3F)$/HSO$_3$F soln	2190			196–198
	$Ag(CO)(zeolite–X)$	2195			221
	$Ag(CO)_2(zeolite–Y)$	2195, 2170			221
	$Ag(CO)(zeolite–Y)$	2170			222
	$Ag(CO)(zeolite–Y)$	2174			223
	$Ag(CO)(zeolite–ZSM-5)$	2185			224
	$Ag(CO)(zeolite–ZSM-5)$	2192			225,226
	$Ag(CO)(H_2O)(zeolite–ZSM-5)$	2181			226
	$Ag(CO)_2(zeolite–ZSM-5)$	2186			225
	$Ag(CO)_2(zeolite–ZSM-5)$	2190(m), 2184(s)			226
	$Ag(CO)(zeolite–A)$	2188			227
	$Ag(CO)^+/SiO_2$	2169			225
	$Ag(CO)^+/SiO_2$	2180–2175			228
	$Ag(CO)^+/TiO_2$	XXX			229
Au^+	$Au(CO)(SO_3F)$	2195			230
	$Au(CO)(SO_3F)$/HSO$_3$F soln	2198			231
	$Au(CO)_2(SO_3F)$/HSO$_3$F soln	2246, 2211			231
	$Au(CO)(HSO_4)$/H$_2$SO$_4$ soln	2194			63
	$Au(CO)_2(HSO_4$/H$_2$SO$_4$ soln	2208			63
	$Au(CO)(OTeF_5)$	2178			217

TABLE V (Continued)

M	Compound or Species[b]	$\nu(CO)^a$ (cm^{-1})	$R(MC)$ (Å)	$R(CO)$ (Å)	References
	Au(CO)Br/CH$_2$Cl$_2$	2159			233
	Au(CO)Cl/CH$_2$Cl$_2$	2162	1.93(2)	1.11(3)	233–236
	Au(CO)Cl/Na(zeolite–Y)	2188			237
	Au(CO)(Tp′)	2144	1.862(9)	1.13(1)	238
	Au(CO)(AuCl$_4$)	2180			233,239
	Au(CO)$_2$(Sb$_2$F$_{11}$)	2254, 2217	1.972(8)	1.11(1)	231,232
	Au(CO)$_3$(Sb$_2$F$_{11}$)	2212			217
	Au(CO)$_2$(UF$_6$)	2200			240

[a] Abbreviations: Tp′ = BH(3,5-(CF$_3$)$_2$Pz)$_3$) (pz = pyrazolyl).
[b] The ν(CO) values in italics are from Raman spectra; all other ν(CO) values are from IR spectra.
[c] The peak at 2138 cm^{-1} may be due to uncomplexed CO.
[d] The formulation of this species as Cu(CO)F may be incorrect. Copper(I) fluoride has not been shown to exist in a condensed phase, despite numerous attempts to prepare it.

TABLE VI

Group 12(IIB) M–CO Species With $\nu(CO) > 2143$ cm^{-1}

M	Compound or Material	$\nu(CO)^a$ (cm^{-1})	$R(MC)$ (Å)	$R(CO)$ (Å)	References
Zn^{2+}	Zn(zeolite–Y) + CO	2218 (2214)			126,241
	ZnO + CO	2212–2169			241–246
	ZnO ($10\bar{1}0$ face) + CO	2202		1.10	247
	$Zn(CO)F_2$	2185			105
Cd^{2+}	Cd(zeolite–Y) + CO	2209			126
Hg_2^{2+}	$Hg_2(CO)_2(Sb_2F_{11})_2$	2248, 2247			248,249
Hg^{2+}	$Hg(CO)_2(Sb_2F_{11})_2$	2281, 2278	2.08(1)	1.104(12)	248,249

^{a}The $\nu(CO)$ values in italics are from Raman spectra; all other $\nu(CO)$ values are from IR spectra.

3. Be^{2+} to Ba^{2+}

Carbon monoxide adsorbed to the 001 face of MgO at 77 K resulted in three $\nu(CO)$ bands (125). These were attributed to three different sites, corner $Mg(CO)O_3$ sites (2203 cm^{-1}), edge or step $Mg(CO)O_4$ sites (2170 cm^{-1}), and face $Mg(CO)O_5$ sites (2157 cm^{-1}), as shown in Fig. 8. Magnesium(II) ions intercalated into zeolite–Y and zeolite–X form carbonyl complexes with $\nu(CO)$ values of 2213 and 2205 cm^{-1}, respectively. Matrix isolated $Ca(CO)F_2$ exhibited $\nu(CO)$ at 2178 cm^{-1} (105). Like magnesium, Ca(zeolite–Y) (2197 cm^{-1}) and Ca(zeolite–X) (2192 cm^{-1}) also adsorb CO but exhibit lower $\nu(CO)$ values. Calcium oxide supported on alumina adsorbs CO and has a $\nu(CO)$ value of 2182 cm^{-1}. The ions Sr^{2+} and Ba^{2+} form complexes similar to those above. While the matrix isolated $M(CO)F_2$ species have similar $\nu(CO)$ values, the M–Y show a decrease in $\nu(CO)$ from Mg^{2+} down

TABLE VII

f-Block M–CO Species With $\nu(CO) > 2143$ cm^{-1}

M	Compound	Conditions	$\nu(CO)^a$ (cm^{-1})	References
Nd^{3+}	$Nd(CO)F_3$	Ar/CO matrix, 10 K	2187	109
	$Nd_2(CO)F_6$	Ar/CO matrix, 10 K	2183	109
Gd^{3+}	$Gd(CO)F_3$	Ar/CO matrix, 10 K	2194	109
	$Gd_2(CO)F_6$	Ar/CO matrix, 10 K	2190	109
Ho^{3+}	$Ho(CO)F_3$	Ar/CO matrix, 10 K	2198	109
	$Ho_2(CO)F_6$	Ar/CO matrix, 10 K	2194	109
Lu^{3+}	$Lu(CO)F_3$	Ar/CO matrix, 10 K	2205	109
	$Lu_2(CO)F_6$	Ar/CO matrix, 10 K	2195, 2103	109
U^{4+}	$U(CO)F_4$	Ar/CO matrix, 12 K	2182	250

^{a}All $\nu(CO)$ values are from IR spectra.

TABLE VIII

Carbon–13 NMR Data of Carbonyl Complexes With High Carbonyl Stretching Frequencies[a]

Compound	Medium	$\delta(^{13}C)^b$	$^1J_{MC}$	$\nu(CO)_{ave}$	$^1K_{MC}$	References
CO	HSO$_3$F or CD$_2$Cl$_2$	184		2143		230,231
CH$_3$CO$^+$	H$_2$SO$_4$	150		2309		143,257
N(CO)$_2$(Sb$_3$F$_{16}$)	CF$_3$CH$_2$CF$_3$	122		2330		151
ClCO$^+$	COCl$_2$/SbF$_5$/ SO$_2$ClF	134		2256^c		152,153,270
BrCO$^+$	Br$_2$/SbF$_5$/SO$_2$ClF	127				270
ICO$^+$	I$_2$/SbF$_5$/SO$_2$ClF	100				270
Na$_2$Hf(CO)$_6$		244		1757^d		35
NaTa(CO)$_6$		211		1850^d		35
Cr(CO)$_6$	Solid	212		2029		260,261
Mo(CO)$_6$	Solid	204		2007		260,261
W(CO)$_6$	Solid	192		2014		260,261
Re(CO)$_6$(Sb$_2$F$_{11}$)	Solid	171		2116		262,263
Fe(CO)$_6$(Sb$_2$F$_{11}$)$_2$	Solid	179		2216		162
Ru(CO)$_6$(Sb$_2$F$_{11}$)$_2$	Solid	166		2216		164
Os(CO)$_6$(Sb$_2$F$_{11}$)$_2$	Solid	147		2211		164
Ir(CO)$_6$(Sb$_2$F$_{11}$)$_3$	Solid	121		2268		173
cis-Pt(CO)$_2$I$_2$	C$_6$D$_6$	154	1521	2131	23.5	184
cis-Pt(CO)$_2$Br$_2$	CH$_2$Cl$_2$/CD$_2$Cl$_2$	153	1563	2150^e	24.1	184
cis-Pt(CO)$_2$Cl$_2$	CH$_2$Cl$_2$/CD$_2$Cl$_2$	152	1569	2156^e	24.2	184
trans-Pt(CO)$_2$I$_2$	C$_6$D$_6$	164	1470	2126^e	22.7	184
trans-Pt(CO)$_2$Br$_2$	CH$_2$Cl$_2$/CD$_2$Cl$_2$	153	1574	2142^e	24.3	184
trans-Pt(CO)$_2$Cl$_2$	SOCl$_2$/CDCl$_3$	157	1565	2150	24.2	184
[NR$_4$][Pt(CO)I$_3$]	CH$_2$Cl$_2$	156	1636	2078	26.7	235
[NR$_4$][Pt(CO)Br$_3$]	CH$_2$Cl$_2$	153	1701	2089	26.2	235
[NR$_4$][Pt(CO)Cl$_3$]	CH$_2$Cl$_2$	152	1732	2098	25.2	235
Pt(CO)$_4$(Pt(SO$_3$F)$_6$)	HSO$_3$F	141	1576(2)	2269	24.3	186
Pt(CO)$_4$(Sb$_2$F$_{11}$)$_2$	Unknown	137	1550	2244	23.9	186
Pd(CO)$_4$(Sb$_2$F$_{11}$)$_2$	Unknown	144		2267		4,181
cis-Pt(CO)$_2$(SO$_3$F)$_2$	Unknown	131	2011	2200	31.0	4,181
cis-Pd(CO)$_2$(SO$_3$F)$_2$	Unknown	145		2218		4,181
Cu(CO)$^+$	BF$_3$·H$_2$O	169		2160		196
Cu(CO)$_3^+$	HSO$_3$F/H$_2$SO$_4$	169		2177		196
Cu(CO)$_4^+$	BF$_3$·H$_2$O	170		2185		196
Ag(CO)(Tp′)	CD$_2$Cl$_2$	175		2178		216
Ag(CO)(OTeF$_5$)	Solid	173	265(12)	2189	−18.8	148
Ag(CO)(B(OTeF$_5$)$_4$)	CD$_2$Cl$_2$	174		2204		148,219
(Ag(CO))$_2$(X)	Solid	171	284(12)	2203	−20.2	148
(Ag(CO))$_2$(Y)	Solid	171	263(12)	2207	−18.7	148
Ag(CO)$_2^+$	HSO$_3$F	172		2190		196–198
(Ag(CO)$_2$)$_2$(X)	Solid	172	203(12)	2197	−14.4	148
(Ag(CO)$_2$)$_2$(Y)	Solid	172	190(12)	2197	−13.5	148
Au(CO)Br	CD$_2$Cl$_2$	174		2159		233
Au(CO)Cl	CD$_2$Cl$_2$	172		2162		233–235
Au(CO)(AuCl$_4$)	CD$_2$Cl$_2$	171		2180^f		233,239
Au(CO)(Tp′)	CD$_2$Cl$_2$	173		2144		238
Au(CO)$^+$	HSO$_3$F/SbF$_5$ 1:1	158				231
Au(CO)(SO$_3$F)	HSO$_3$F	162		2198		231

(continues)

TABLE VIII (*Continued*)

Compound	Medium	$\delta(^{13}C)^b$	$^1J_{MC}$	$\nu(CO)_{ave}$	$^1K_{MC}$	References
$Au(CO)_n^+$ $(n = 1, 2)$	HSO_3F/SbF_5	167				231
$Au(CO)_2(Sb_2F_{11})$	Solid^g	174		2236		231,232
$Hg_2(CO)_2(Sb_2F_{11})_2$	Solid	189	$3350(20)^h$	2248	61.9	248,249
$Hg(CO)_2(Sb_2F_{11})_2$	Solid	169	5219(5)	2280	96.5	248,249
	Magic acid	171		2280		248,249
$Co(CO)_4^-$	HSO_3F	182		2153		167
$Rh(CO)_4^-$	HSO_3F	172		2169		167
$Pt_2(CO)_6^{2+}$	H_2SO_4	166 (a)^i	200	2197	3.1	418
		159 (e)^i	−26		−0.40	
$Pd_2(CO)_2^{2+}$	H_2SO_4/1-hexene	177		2156		63

^{a}The units: $\delta(^{13}C)$, ppm from $SiMe_4$; $^1J_{MC}$, Hz; $\nu(CO)_{ave}$, cm^{-1}; $^1K_{MC}$, × 10^{21} N A^{-2} m^{-3}. Abbreviations: Tp′ = HB[3,5-(CF$_3$)$_2$Pz]$_3$ (Pz = pyrazolyl); X = [Zn(OTeF$_5$)$_4$]$^{2-}$; Y = Ti(OTeF$_5$)$_6^{2-}$.
^{b}Error ≤ 1 ppm.
^{c}(Sb$_n$F$_{5n+1}$) $(n > 2)$.
^{d}The T_{1u} values.
^{e}sym-C$_2$H$_2$Cl$_4$.
^{f}SOCl$_2$.
^{g}The same $\delta(^{13}C)$ was observed in HSO$_3$F, 1:1 HSO$_3$F/SbF$_5$, and SO$_2$.
^{h}$^2J_{MC}$ = 850(50) Hz.
^{i}Axial - a, equatorial = e.
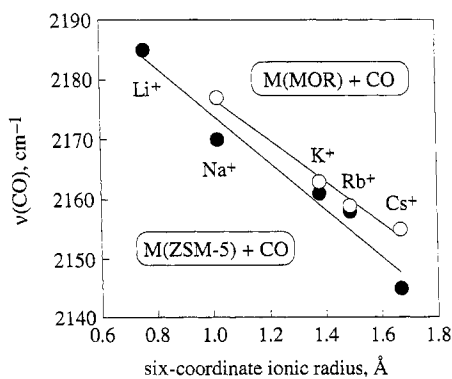

Figure 6. The ν(CO) values for two alkali metal substituted zeolites, mordenite and ZSM-5. The lines are linear least-squares fits to the data.

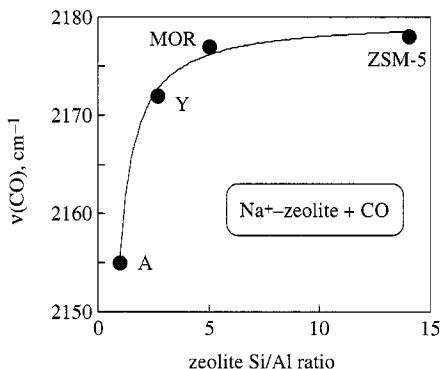Figure 7.   Dependence of ν(CO) for Na(CO)$^+$–zeolite materials on the Si/Al ratio of the zeolite. Only those values from Table I that correspond to near-zero coverage are included in this plot.

the group to Ba^{2+} (2178 cm^{-1}). The only s-block metal carbonyls that can be generated in fluid solution are Ca(CO)(Cp*)$_2$ and Sr(CO)(Cp*)$_2$ (127). Both of these were generated by treating toluene solutions of the corresponding M(Cp*)$_2$ compounds with elevated pressures of gaseous CO.

B. p-Block Species

1.   Boranes

All of the compounds with ν(CO) > 2143 cm^{-1} listed in this category in Table II are neutral compounds (128–150). Both BH$_3$(CO) and B$_2$H$_4$(CO)$_2$, the latter with an ethane-like structure, contain tetrahedral boron atoms with four $2c$–$2e$ bonds. The remaining compounds contain boron atoms with more than four bonds,
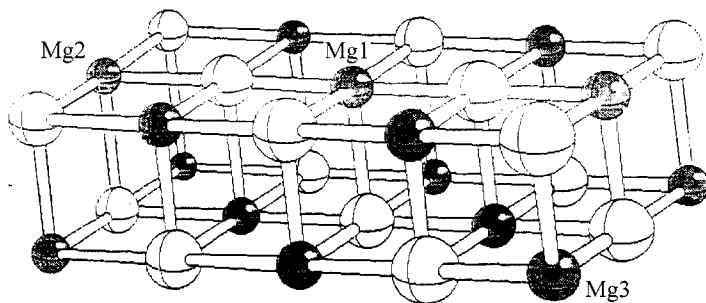

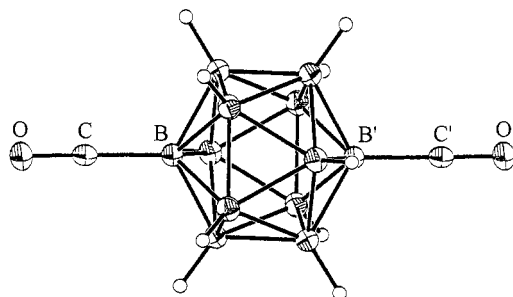Figure 8.   Idealized relaxed 001 surface of MgO, showing three different Mg^{2+} sites.

Figure 9. Structure of 1,12-$B_{12}H_{10}(CO)_2$ (50% probability ellipsoids except for H atoms). Selected interatomic distances (Å) and angles (deg): C–O, 1.119(2); C–B, 1.543(2); O–C–B, 179.1(1).

that is, with some $3c$–$2e$ bonds. The structure of one of these, 1,2-$B_{12}H_{10}(CO)_2$ [$\nu(CO) = 2210$ cm^{-1}], is shown in Fig. 9 (135, 136). Note that the anionic cluster 2-$B_{10}H_9(CO)^-$ has a $\nu(CO)$ value 18 cm^{-1} below the similar but neutral cluster $B_{10}H_8(CO)_2$.

2. Al^{3+}

The Lewis acid AlMe$_3$ forms a complex with CO in a neat CO matrix. The resultant species, AlMe$_3$(CO) (138), has a $\nu(CO)$ value of 2185 cm^{-1}, 18 cm^{-1} higher than BH$_3$(CO). Carbon monoxide also interacts with Al^{3+} ions in various aluminas. In many cases, more than one Al–CO species is observed for a given sample, which is commensurate with different types of Al^{3+} sites and is similar to what was observed for CO adsorbed on MgO (see above). The range of $\nu(CO)$ values given in Table II for Al$_2$O$_3$ + CO, 2238–2150 cm^{-1}, demonstrates the range of Al–CO interactions that are possible at different aluminum sites within a given alumina and for different aluminas that have been studied (e.g., α-Al$_2$O$_3$, γ-Al$_2$O$_3$, and δ,θ-Al$_2$O$_3$).

3. R^+

Acylium ions such as CH$_3$CO$^+$ and (CH$_3$)$_2$CHCO$^+$ are important reaction intermediates in a number of organic reactions and have been studied by a variety of techniques (268). These two ions are the only ones for which structural data *and* $\nu(CO)$ values are available. During our investigation of Ag(I) carbonyls (148), we decided to redetermine the structure of [CH$_3$CO][SbCl$_6$] so that, with modern X-ray diffraction equipment and low-temperature data collection, the $R(CO)$ value for at least one acylium ion would be known with good precision. We discovered that earlier investigators (147) had overlooked the alternative, and more appropriate,

space group that would require that the CH_3CO^+ cation be disordered about a crystallographic inversion center. We did not reinvestigate the structure of $[CH_3CO][SbF_6]$, but it is possible that the cation in this structure is disordered as well. Instead, we reinvestigated the structure of $[(CH_3)_2CHCO][SbCl_6]$ (143 K data collection) (148), which had been reported in 1972 (room temperature data collection) (147), and found the $R(CO)$ value to be 1.101(4) Å [the $R(CO)$ value reported in 1972 was 1.116(10) Å]. The structure of the isopropylium cation is shown in Fig. 10. This is one of the few cases where it is has been demonstrated that a $\nu(CO)$ value > 2143 cm^{-1} results in a $R(CO)$ value < 1.12822 Å.

4. Si^{4+}

No molecular species of Si(IV) with $\nu(CO)$ > 2143 cm^{-1} have been reported. Silicon dioxide, however, adsorbs CO; the resulting species exhibits a $\nu(CO)$ stretch of 2158 cm^{-1} (124).

5. Sn^{2+} and Pb^{2+}

Monomeric Sn(II) and Pb(II) halides were cocondensed with CO in an argon matrix at 10 K (150). The species $M(CO)X_2$ all exhibited $\nu(CO)$ values > 2143 cm^{-1}. For the $Pb(CO)X_2$ species, $\nu(CO)$ decreased in the order F (2176 cm^{-1}) > Cl (2175 cm^{-1}) > Br (2161 cm^{-1}) > I (~2149 cm^{-1}).
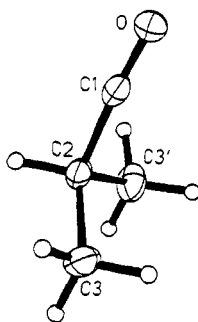

Figure 10.   Structure of the $(CH_3)_2CHCO^+$ cation. Selected distances (Å) and angles (deg): C1–O, 1.101(4); C1–C2, 1.458(4); C2–C3, 1.538(3); C2–C1–O, 1.774(3). [Reprinted with permission from P. K. Hurlburt, J. I Rack, J. S. Luck, S. F. Dec, J. D. Webb, 0. P. Anderson, and S. H. Strauss, *J. Am. Chem. Soc., 116*, 10003 (1994). Copyright © 1994 American Chemical Society.]

6. N^+

The remarkable salt $[N(CO)_2][Sb_3F_{16}]$ was recently reported by Seppelt and co-workers (151). The $N(CO)_2^+$ cation, which is isoelectronic with the equally remarkable N_5^+ cation recently reported by Christe et al. (269), is bent, with a C–N–C bond angle of 130.7(3)° and nearly linear N–C≡O linkages. The C–O bond distances are 1.118(4) Å and 1.114(5) Å and the average $\nu(CO)$ value is 2340 cm^{-1} (151). As far as we know, this is the highest $\nu(CO)$ value reported for any chemical species.

7. Cl^+

The ClCO$^+$ cation, generated in superacid solution in 1991 (270), was recently characterized by infrared (IR) spectroscopy [$\nu(CO) = 2256$ cm^{-1}] (152, 153). This species is believed to be important in Friedel–Crafts reactions of carbonyl halides and also as a gas-phase species in plasma etching processes.

C. Groups 3 (IIIB)–7 (VIIB) d-Block Species

1. Sc^{3+}, Y^{3+}, and La^{3+}

A number of argon matrix isolated group 3 (IIIB) metal carbonyl complexes exist. The complex with the highest $\nu(CO)$ value is Sc(CO)O$^+$, with $\nu(CO) = 2222$ cm^{-1}. Many of the other species in this group are fluorides of the form M(CO)F$_2$ or M$_2$(CO)F$_6$. In each case, the mononuclear species have a higher $\nu(CO)$ value than the dinuclear species; for La^{3+} the $\nu(CO)$ difference is 63 cm^{-1}. For both series, there is a $\nu(CO)$ trend: Sc^{3+} > Y^{3+} > La^{3+}. In addition, CO forms an adduct with La$_2$O$_3$ with $\nu(CO) = 2170$ cm^{-1} at low coverage (255, 256).

2. Ti^{3+}, Ti^{4+}, and Zr^{4+}

Carbonyl complexes of titanium with $\nu(CO) > 2143$ cm^{-1} existing in two different oxidation states have been reported. The cationic complex [Ti(CO)O]$^+$ (argon matrix) has been isolated and exhibits a $\nu(CO)$ value of 2143 cm^{-1}. Titanium(IV) carbonyl species are limited to CO adsorbed on TiO$_2$ or on modified TiO$_2$ surfaces. The carbonyl stretching frequency is dependent on the form of TiO$_2$ used. The rutile form of TiO$_2$ has $\nu(CO) = 2182$ cm^{-1}, while the anatase form exhibits $\nu(CO)$ values in the range 2178–2184 cm^{-1} (156–158). Silicon doped TiO$_2$ (TiO$_2$/SiO$_2$) shows a range of $\nu(CO)$ values, 2178–2184 cm^{-1}, which is comparable to the range for the anatase form of TiO$_2$ (2180–2188 cm^{-1}) (158). Zirconium(IV) oxide also forms surface carbonyl complexes that have an intense, broad $\nu(CO)$ band centered at ~2190 cm^{-1} (159). Sulfate-loaded ZrO$_2$ (sd-ZrO$_2$) also takes up CO, with multiple $\nu(CO)$ peaks in the range 2170–2220 cm^{-1} (159). In the

doped materials, the degree of sulfate loading affected peak positions and intensities, except for the highest frequency peak, 2220 cm^{-1}, the position of which remained constant at different sulfate loadings. The nonclassical molecular carbonyl cations O-inside-Zr(CO)(Cp*)$_2$(COCH$_3$)$^+$ and O-inside-Zr(CO)(Cp)$_2$(COCH$_3$)$^+$ have ν(CO) values of 2152 and 2176 cm^{-1}, respectively (160). The structure of the O-outside-Zr(CO)(Cp*)$_2$(COCH$_3$)$^+$ cation is shown in Fig. 11.

3. V^{3+}

Only one high stretching frequency V(III) carbonyl complex has been reported. The cationic complex [V(CO)O]$^+$ has been isolated in an argon matrix at 12 K and has a ν(CO) value of 2205 cm^{-1}.

4. Cr^{2+} and Cr^{3+}

Carbonyl complexes of chromium in two different oxidation states have been reported. The Cr(II) complex Cr(CO)F$_2$, ν(CO) = 2185 cm^{-1}, has been generated in an Ar/CO matrix (105). No molecular forms of Cr(III) carbonyls are known to exist. Three different species of CO adsorbed onto Cr$_2$O$_3$ are known: bulk Cr$_2$O$_3$
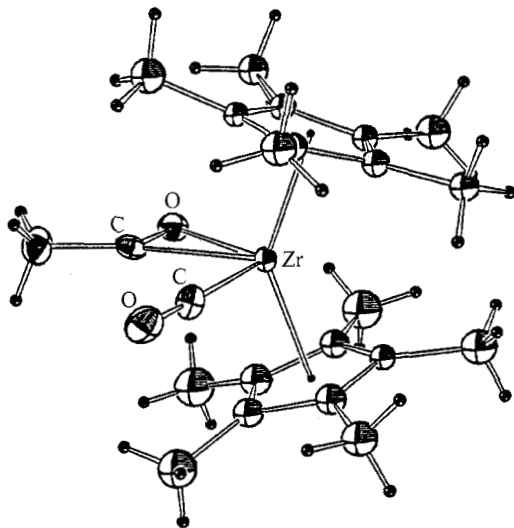

Figure 11.   Structure of the "O-outside" isomer of the Zr(Cp*)$_2$ (η^2-CH$_3$CO)(CO)$^+$ cation.